Acta Cryst. (1998). D**54**, 378–385

Structure Analysis of Two CheY Mutants: Importance of the Hydrogen-Bond Contribution to Protein Stability

DEBORAH WILCOCK,[a] MARÍA TERESA PISABARRO,[b] EVA LÓPEZ-HERNANDEZ,[b] LUIS SERRANO[b] AND MIQUEL COLL[a]*

[a]*Departament de Biologia Molecular i Cel·lular, Centre d'Investigació i Desenvolupament-CSIC, Jordi Girona 18–26, 08034 Barcelona, Spain, and* [b]*European Molecular Biology Laboratory, Meyerhofstrasse 1, 6900 Heidelberg, Germany. E-mail: mcccri@cid.csic.es*

(*Received 17 June 1997; accepted 15 September 1997*)

Abstract

The crystal structures of two double mutants (F14N/V21T and F14N/V86T) of the signal transduction protein CheY have been determined to a resolution of 2.4 and 2.2 Å, respectively. The structures were solved by molecular replacement and refined to final R values of 18.4 and 19.2%, respectively. Together with urea-denaturation experiments the structures have been used to analyse the effects of mutations where hydrophobic residues are replaced by residues capable of establishing hydrogen bonds. The large increase in stabilization (-12.1 kJ mol^{-1}) of the mutation Phe14Asn arises from two factors: a reverse hydrophobic effect and the formation of a good N-cap at α-helix 1. In addition, a forward–backward hydrogen-bonding pattern, resembling an N-capping box and involving Asn14 and Arg18, has been found. The two Val to Thr mutations at the hydrophobic core have different thermodynamic effects: the mutation Val21Thr does not affect the stability of the protein while the mutation Val86Thr causes a small destabilization of 1.7 kJ mol^{-1}. At site 21 a backward side-chain-to-backbone hydrogen bond is formed inside α-helix 1 with the carbonyl O atom of the $i-4$ residue without movement of the mutated side chain. The destabilizing effect of introducing a polar group in the core is efficiently compensated for by the formation of an extra hydrogen bond. At site 86 the new O^{γ} atom escapes from the hydrophobic environment by a χ_1 rotation into an adjacent hydrophilic cavity to form a new hydrogen bond. In this case the isosteric Val to Thr substitution is disruptive but the loss in stabilization energy is partly compensated by the formation of a hydrogen bond. The two crystal structures described in this work underline the significance of the hydrogen-bond component to protein stability.

1. Introduction

The energetic contribution of hydrogen bonds to protein folding and stability has previously been a subject for discussion (Dill, 1990; Creighton, 1991; Pace *et al.*, 1996; Shirley *et al.*, 1992; Byrne *et al.*, 1995). A useful method to study their significance is to analyse designed mutants where the substitutions introduce new hydrogen bonds. However, the limited number of studies, which are confined to a few protein case studies, might be misleading because of possible side effects, other than the new hydrogen-bond formation, in the particular local environment of the substitution site. One way to reduce such spurious effects is to make the mutation isosteric, as in the case of the substitution of Val by Thr. This mutation should produce a very minor change in the volume and geometry of the mutated position and should not leave a cavity. There are two destabilizing effects on mutating Val to Thr, one that involves a change in the van der Waals interactions of the C^{γ} with the rest of the protein and the other the burial of the side-chain $O^{\gamma 1}$ group of the Thr residue. The final outcome will depend on the packing of the C^{γ} atoms, their exposure to the solvent and the availability of any donor or acceptor groups for the $O^{\gamma 1}$ group in the protein (Byrne *et al.*, 1995; Serrano *et al.*, 1992; Blaber *et al.*, 1993). The experimental $\Delta\Delta G$ values from these studies vary between 3.3 and 13.3 kJ mol^{-1} (0.8 and 3.2 kcal mol^{-1}). In the case of the three buried Val residues of T4 lysozyme the three-dimensional structure of the corresponding Thr mutants have been obtained by X-ray diffraction analysis (Blaber *et al.*, 1993). For these mutants it was found that the newly introduced hydroxyl group was making hydrogen bonds to either protein groups [$\Delta\Delta G = -5.4$ kJ mol^{-1} (-1.3 kcal mol^{-1})] or to a newly buried water molecule [$\Delta\Delta G = -11.7$ kJ mol^{-1} (-2.8 kcal mol^{-1})] (Blaber *et al.*, 1993). These studies suggested that the energy cost of burying a polar group in an enviroment in which no hydrogen bond is possible could be substantially more than the value of 11.7 kJ mol^{-1} (2.8 kcal mol^{-1}).

In a recent study characterizing the structure of the transition state for unfolding of the chemotactic protein from *E. coli*, CheY by the protein engineering method (López-Hernandez & Serrano, 1996), several Val–Thr mutations were made. All these mutants were performed in addition to the single point mutation Phe14Asn. This mutation was initially designed to

Table 1. *Crystal data and refinement statistics for the mutants 1 and 2*

	Mutant 1	Mutant 2
(*a*) Crystal data		
a (Å)	54.31	54.07
b (Å)	54.31	54.07
c (Å)	91.83	91.72
Space group	$P3_1$	$P3_1$
(*b*) Data collection		
Total No. of reflections	82839	25441
No. of unique reflections	11899	13544
No. of unique reflections > 3σ	9475	10496
R_{merge} (%)†	8.8	4.8
Redundancy	6.9	1.8
Completeness (%)	92.1	86.0
Last shell completeness (resolution) (%)	64.6 (2.55–2.4 Å)	55.6 (2.34–2.2 Å)
(*c*) Refinement		
R (%)‡	18.4	19.7
R_{free} (%)§	26.4	28.0
Resolution (Å)	10.0–2.4	10.0–2.2
No. of unique reflections > 2σ	10044	11179
R.m.s. Δ bonds (Å)	0.009	0.008
R.m.s. Δ angles (°)	1.5	1.4
Isotropic thermal factor restraints (r.m.s. σ)		
Main-chain bond (Å)	3.59 (1.5)	2.84 (1.5)
Main-chain angle (°)	5.33 (2.0)	4.41 (2.0)
Side-chain bond (Å)	5.96 (2.0)	4.69 (2.0)
Side-chain angle (°)	8.76 (2.5)	7.07 (2.5)

† $R_{merge} = \sum_{h,k,l}\sum_i I_i(h,k,l) - |I(h,k,l)| / \sum_h \sum_i I_i(h,k,l)$, where (h,k,l) are the unique reflections, $I_i(h,k,l)$ is the ith measurement intensity of reflection h,k,l and $|I(h,k,l)|$ is the mean of all measurements h,k,l. ‡ $R = \sum_{h,k,l}||F_{obs}(h,k,l)|-|F_{calc}(h,k,l)| / \sum_{h,k,l}|F_{obs}(h,k,l)|$, where $F_{obs}(h,k,l)$ and $F_{calc}(h,k,l)$ are the observed and calculated structure factors, respectively. § R_{free} is the R value calculated for a subset of 10% of randomly selected reflection not used in the refinement.

stabilize the protein in order to introduce other destabilizing mutations (Muñoz *et al.*, 1994). Interestingly, one of those mutants, Phe14Asn/Val21Thr, was as stable as the reference protein (Phe14Asn, pseudo wild type), even though Val21 is buried in the wild-type structure. To find out the reasons for the apparent lack of destabilization we have crystallized and determined the three-dimensional structure of this double mutant. We have also mutated another buried Val residue (Val86), on the pseudo wild type and found again that only a small destabilization was produced. The three-dimensional structure of this mutant has also been determined. The crystal structures here analysed show two different ways of compensating the loss in stabilization caused by the $-CH_3$ to $-OH$ substitution in the protein core and indicate the significance of the hydrogen-bond component on protein stability.

2. Materials and methods

2.1. *Urea denaturation curves*

The urea denaturation experiments were carried out as previously described (López-Hernandez & Serrano, 1996; Muñoz *et al.*, 1994; Filimonov *et al.*, 1993). The unfolding reaction was monitored by recording the fluorescence emission at 315 nm upon excitation at 290 nm in an AB2 SLM Aminco–Bowman spectrofluorometer. Experimental data from four different experiments performed on different days were averaged and the average fitted to equation (1).

$$F = \{(F_N + a[\text{denaturant}]) + (F_U + b[\text{denaturant}]) \times \exp(m[\text{denat}] - \Delta G_{H_2O})/RT\} \div \{1 + \exp(m[\text{denat}] - \Delta G_{H_2O})/RT\}, \quad (1)$$

where F is the fluorescence emission of the protein, F_N is the fluorescence of the folded state and F_U of the unfolded state. The dependence of the intrinsic fluorescence upon denaturant concentrations, in both the native and the denatured states, is taken into account by the terms of a[urea] and b[urea], respectively, where a and b are constants.

2.2. *Crystallization, data collection and processing*

Both mutant proteins were crystallized by the hanging-drop method using high concentrations of ammonium sulfate (2.6–3.0 *M* in Tris–HCl buffer at pH 7.2) at 293 K. Droplets consisting of 4 µl of protein, at a concentration of 2 mg ml^{-1} and 2 µl of precipitant were equilibrated against a 1 ml reservoir. Crystals appeared after approximately 2 d and grew to a suitable size for data collection after a further 5 d.

For mutant 1, data were collected on a Mar Research image-plate detector using a Rigaku RU200 rotating anode to a maximum resolution of 2.4 Å. The protein crystallized in space group $P3_1$ with two molecules in

the asymmetric unit and unit-cell dimensions of $a = b = 54.31$ and $c = 91.83$ Å. For mutant 2, data were collected on a Mar Research image-plate detector using an Elliot GX21 rotating-anode generator with a graphite monochromator to a resolution of 2.2 Å. This mutant crystallized isomorphously with the first in $P3_1$ with unit-cell dimensions, $a = b = 54.07$ and $c = 91.72$ Å and two molecules in the asymmetric unit. Two crystals were used in the data collection of mutant 1 and both data sets were processed with *DENZO* and scaled with *SCALEPACK* (Otwinowski, 1993). The data for mutant 2 were processed with *XDS* (Kabsch, 1988). Data statistics are given in Table 1.

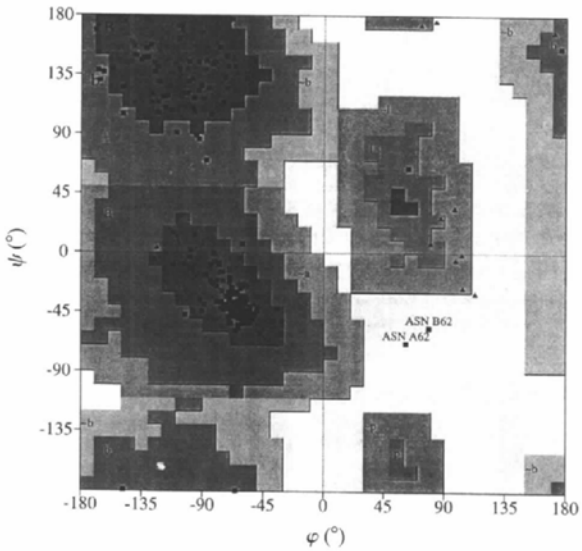

(*a*)

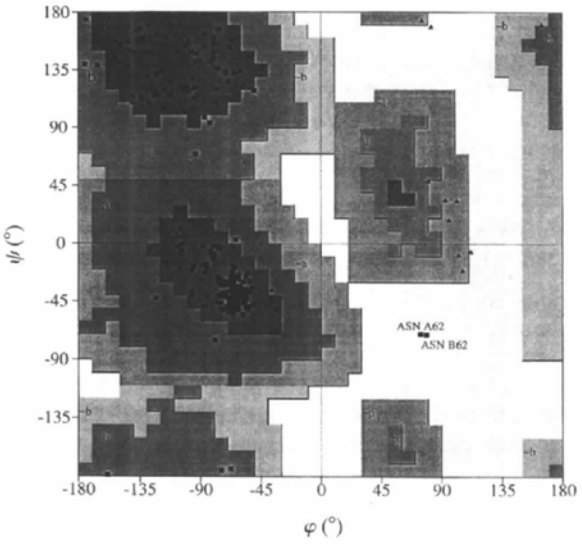

(*b*)

Fig. 1. Final Ramachandran plots for mutant 1 (*a*) and mutant 2 (*b*). Triangles indicate glycine residues, squares non-glycine residues.

Table 2. *Thermodynamic analysis of the different mutant proteins*

	$1/2[\text{urea}]_{eq}$†	m‡	ΔG_{eq}§
F14N¶	4.68	7.5 ± 0.2	35.1 ± 0.8
Mutant 1¶	5.03	6.9 ± 0.2	34.7 ± 0.8
Mutant 2	4.44	7.5 ± 0.2	33.4 ± 0.8

† Urea concentration at which half of the protein is denatured as measured in equilibrium. ‡ Slope of the equilibrium denaturation curves in kJ mol^{-1} M^{-1}. § Free energy in kJ mol^{-1} of unfolding in water, obtained by fitting the curves to a two-state transition, as indicated in Filimonov *et al.* (1993). ¶ The data for the F14N and mutant 1 (only the unfolding data), has been previously published and it is shown here for comparative purposes.

2.3. *Structure determination and refinement.*

The two mutant structures were determined by the molecular replacement method using the apo-CheY structure from *E. coli* (Volz & Matsumura, 1991) as a starting model (Brookhaven Protein Data Bank, entry 3CHY). The rotation and translation functions were calculated with *AMoRe* (Navaza, 1994), together with preliminary rigid-body refinement using the *FITING* option. For mutant 1 this resulted in a correlation coefficient of 73.4% and an R factor of 32.0%. For mutant 2 the correlation factor was 68.1% and the R factor 30.2%. The mutated residues were set in the initial models as dummy atoms with zero occupancies. The appropriate side chains were modelled based on the residual electron density clearly visible in both $2F_o - F_c$ and $F_o - F_c$ maps at the mutation sites. Refinement was then continued with *X-PLOR* (Brünger, 1992*a*), slowly increasing the resolution from 3.0 Å to the final values of 2.4 and 2.2 Å for the respective mutants. Simulated-annealing cycles were included in the refinement and were interspersed with frequent inspections of the $2F_o - F_c$ and $F_o - F_c$ maps using *TURBO-FRODO* (Rousell & Cambillau, 1991). During the refinement process 10% of the reflections were set aside for the R_{free} calculation (Brünger, 1992*b*). Once the highest resolution data had been incorporated a B-factor refinement was carried out with restraints imposed on atoms directly bonded. A search for water molecules was then initiated. The water molecules were treated in the refinement as solvent O atoms. The criteria for location of a water molecule were (i) a well shaped peak in the difference map at hydrogen-bond distance from a possible hydrogen-bonding partner; (ii) retention of a satisfactory geometry during refinement and (iii) a final B value of less than 70 $Å^2$. The two molecules found in the asymmetric unit of both mutants were refined independently throughout. The final R factors are 18.4% ($R_{free} = 26.4\%$) for mutant 1 and 19.7% ($R_{free} = 28.0\%$) for mutant 2. The final mean overall B values are 32.0 $Å^2$ for protein atoms and 41.6 $Å^2$ for solvent atoms in mutant 1, and 35.5 and 48.2 $Å^2$ for mutant 2, respectively. The final structures consist of 125 protein residues out of 129 amino acids of the chemical

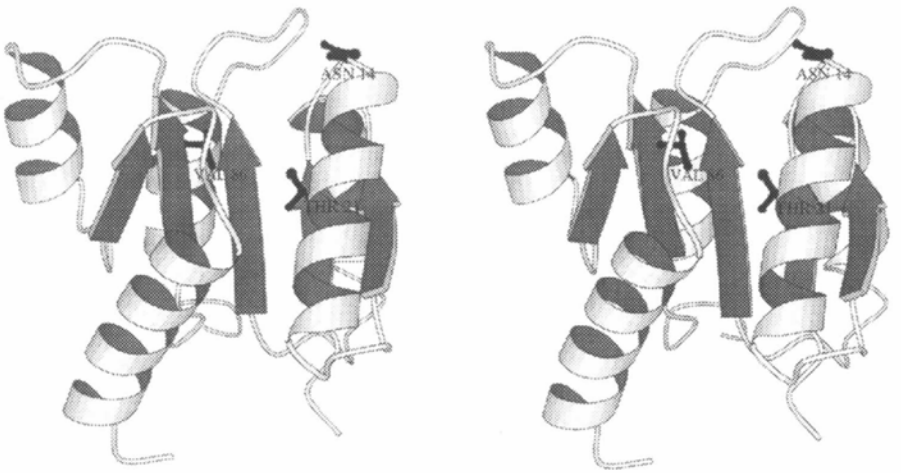

Fig. 2. Stereo *MOLSCRIPT* (Kraulis, 1991) plot of mutant 1 showing the positions of the mutated residues, Phe14Asn and Val21Thr. Mutant 2 includes the mutations Phe14Asn and Val86Thr.

sequence and 45 solvent molecules for mutant 1 and 125 protein residues out of 129 amino acids of the chemical sequence and 41 solvent molecules for mutant 2. The molecular models show good geometry as verified with *PROCHECK* (Laskowski *et al.*, 1993) and the final Ramachandran plots are shown in Fig. 1. Asn62 has a positive φ value because of the classic γ-turn found between residues Pro61 and Met63 (Volz & Matsumura, 1991). The atomic coordinates and structure factors have been deposited with the Brookhaven Protein Data Bank.† Overall solvent accessibilities for the mutated residues were calculated using *X-PLOR* (Brünger, 1992*a*).

3. Results

3.1. *Description of the mutants*

CheY is a small 129-residue protein which functions as the response regulator in the signal-transduction system for bacterial chemotaxis (Stock *et al.*, 1990; Bourret *et al.*, 1991). It is a particularly good model for folding and stability studies as it is small and folds in a regular manner. High-resolution X-ray (Stock *et al.*, 1992; Volz & Matsumura, 1991; Bellsolell *et al.*, 1994) and NMR (Bruix *et al.*, 1993; Santoro *et al.*, 1995) studies are available and thermodynamic (Filimonov *et al.*, 1993) and kinetic (Muñoz *et al.*, 1994) characterizations have been carried out. Several mutant proteins have also been characterized by X-ray diffraction (Cronet *et al.*, 1995; Bellsolell *et al.*, 1996). CheY folds in a $(\beta/\alpha)_5$ manner with the five β-strands forming a central parallel β-sheet surrounded on both sides by five α-helices. The sheets and helices alternate along the primary sequence and the topology of the β-sheet is $\beta2\beta1\beta3\beta4\beta5$. The three substitutions described in this work are located at the N-terminal end of α-helix 1 (Phe14Asn), in the middle of α-helix 1 (Val21Thr) and at the end of β-sheet 4 (Val86Thr) (Fig. 2). Both Val side chains are completely buried (solvent accessibilty for Val21 is 1.40% and for Val86 1.57%) while that of Phe14 is completely solvent-exposed with an overall accessible surface area of 44.04% and occupies the N-cap position of α-helix 1. In CheY, Phe14 is at the active-site area, interacting with the Mg^{2+} cluster when the essential metal binds to the protein (Bellsolell *et al.*, 1996) and its position is related to functional aspects of the protein. For reasons of simplicity, we will denominate mutant Phe14Asn as pseudo wild type, mutant Phe14Asn/Val21Thr as mutant 1 and mutant Phe14Asn/Val86Thr, as mutant 2.

3.2. *Free-energy determination for the Phe14Asn/Val86Thr mutant*

The purified mutant 2 protein eluted on a molecular-weight column as a monomer (data not shown). The denaturation curves were repeated twice and analysed as indicated in methods. In Fig. 3 we show the urea denaturation curve of mutant 2 and that of the pseudo-wild-type protein as a reference. Determination of the thermodynamic parameters shows that mutating Val86 into Thr produces a small destabilization of $\sim$1.7 kJ mol^{-1} ($\sim$0.4 kcal mol^{-1}). The slope m does not change (Table 2), indicating that the difference in solvent accessibility between the native and denatured states is the same as that in the pseudo wild type.

3.3. *Comparison of the mutant structures with the apo-CheY structure*

Table 1 shows the crystal data and refinement statistics for mutants 1 and 2. The global fold of these

† Atomic coordinates and structure factors have been deposited with the Protein Data Bank, Brookhaven National Laboratory (Reference: 1AB5, R1AB5SF, 1AB6, R1AB6SF). Free copies may be obtained through The Managing Editor, International Union of Crystallography, 5 Abbey Square, Chester CH1 2HU, England (Reference: LI0266).

Table 3. *Main- and side-chain torsion angles for wild-type (pdb code 3CHY [13]) and mutant proteins*

Protein	Amino acid	χ (°)	ψ (°)	χ_1 (°)
Wild type	Phe14	−107.6	115.3	−72.2
	Val21	−58.4	−48.8	172.5
	Val86	−111.1	135.5	179.8
Mutant 1	AsnA14	−94.0	112.9	180.0
	ThrA21	−57.6	−46.4	−176.7
	AsnB14	−78.7	109.9	−168.1
	ThrB21	−62.9	−50.2	−175.4
Mutant 2	AsnA14	−96.5	106.3	176.1
	ThrA86	−101.5	139.7	67.3
	AsnB14	−83.9	104.9	176.9
	ThrB86	−108.8	171.7	56.2

proteins is similar to that of the apo-CheY structure (Volz & Matsumura, 1991). For mutant 1 (molecule *A*) the r.m.s. difference with the apo structure for the C^{α} atoms was 0.7 and 1.1 Å for all atoms, with maximum displacements of 3.4 and 7.1 Å. The largest differences are found in the loop region between β-strand 4 and α-helix 4 (residues 89–93). The r.m.s. difference between 3CHY and mutant 2 (molecule *A*) for the C^{α} atoms is 0.6 Å and for all atoms 1 Å. The maximum displacements for each are 2.6 and 7.5 Å, respectively, both of which are located again in the loop region between β-strand 4 and α-helix 4. This region is extensively disordered with complete breaks in the density at some points. Such disorder was a feature of previous CheY mutant structures (Cronet *et al.*, 1995; Bellsolell *et al.*, 1996) and was also seen in the NMR structure (Bruix *et al.*, 1993; Santoro *et al.*, 1995).

3.3.1. *Mutation Phe14Asn.* This mutation is present in both mutants 1 and 2. The new asparagine group is bent around to form a good N-helix cap of α-helix 1. Despite the small differences owing to the environment, in all four molecules the mutation Phe14Asn causes the following structural effects. (i) The mutation does not affect the position or length of α-helix 1, which starts with a 3_{10}-like turn including a three-centered hydrogen bond from O Asn14 to N Met17 and N Arg18. Neither does it affect the position of the main chain at position 14. (ii) The side-chain torsion angles χ_1 and χ_2 of residue 14 change (Table 3), implying that this side chain turns over the cylinder of the helix, capping it by making a bifurcated hydrogen bond from $O^{\delta 1}$ Asn14 to N Thr16 and N Met17. Thus, out of the three hydrogen-bond donors unsatisfied in the wild-type structure, two are now satisfied: the amide N atoms of residues $n + 2$ and $n + 3$, the former being stronger. The side chain of Asn14, lying in the helical path, perfectly mimics a main-chain peptide. Extension of the helix by one residue in a modelling study results in the superposition of the amide N(13) and O(13) with the side-chain atoms $N^{\delta 1}$ and $O^{\delta 1}$ of Asn14 (data not shown). (iii) Asn14 (mutant) is less solvent exposed at 22.7% than Phe14 (wild type) since it is bent over the N-terminus of the helix. (iv) Also, while the side chain of Asn14 hydrogen bonds the main-chain N atom of residues $n + 2$ and $n + 3$, the long side chain of residue $n + 4$, Arg18, hydrogen bonds the main-chain carbonyl group of residues $n - 1$, Asp13 (Fig. 4).

3.3.2. *Mutation Val21Thr.* This mutation is present only in mutant 1. Thr21 essentially superimposes on the valine residue found in the wild-type structure. The new hydroxyl group is readily accommodated in the core of the protein because it can form a hydrogen bond with the carbonyl O atom of Met17, a residue at one-turn ($i - 4$) distance from Thr21 in α-helix 1. The carbonyl O Met17 atom is now, therefore, establishing a bifurcated hydrogen bond with both N Thr21 and O^{γ} Thr21 (Fig. 5). The only discernible movement caused by this mutation is the displacement of the side chain of Met17, which moves away from the newly introduced polar atom O^{γ} Thr21. The solvent accessibility of the Val and Thr side chains are the same (1.4 and 1.5%, respectively).

3.3.3. *Mutation Val86Thr.* This mutation is present in mutant 2. Residue 86 is positioned at the bottom of the cleft between the loops from $\beta 1$ to α-helix 1 and $\beta 3$ to α-helix 3, close to the active site. Although part of the hydrophobic core, there is a water molecule present in both the wild type and mutant structures in this region. In this mutant the Thr86 side chain superimposes its C^{β} on the position previously occupied by the C^{β} of Val86 residue, but the $\chi 1$ torsion angle turns from *gauche*$^+$ to *gauche*$^-$ (Table 3). This keeps the $C^{\gamma 2}$ atom in the same hydrophobic environment as before but the $O^{\gamma 1}$ atom moves into a more hydrophilic cavity, away from the hydrophobic location occupied by $C^{\gamma 1}$ in the wild-type

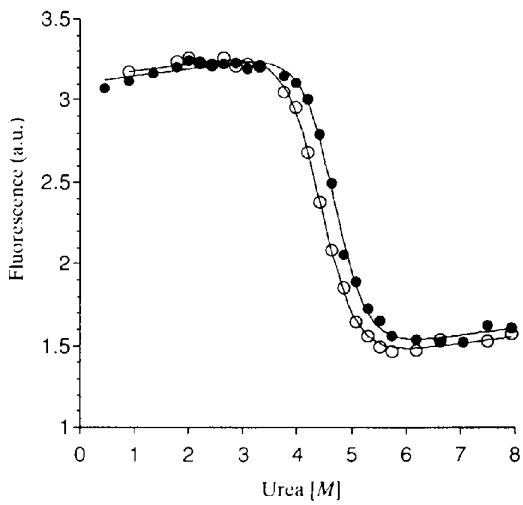

Fig. 3. Urea denaturation of mutant 2 protein. Each curve represents the normalized data of two experiments performed on two different days. The empty circles are for the mutant 2 protein, the filled circles for the pseudo wild-type protein (Phe14Asn), shown here for comparative purposes. The experiments were performed at 298 K, in 50 m*M* Na-Pipes buffer pH 7.

structure (Fig. 6). The hydrophilic cavity is now partially filled as a result of both the rotation of the $O^{\gamma 1}$ atom and the displacement of the methylene side-chain atoms of Lys109. In its new position, the $O^{\gamma 1}$ atom of Thr86 can form a bifurcated hydrogen bond with the $O^{\delta 2}$ Asp57 and a water molecule (W32). This solvent molecule was previously coordinated to $O^{\delta 1}$ Asp57 and $O^{\delta 2}$ Asp12. After the mutation it maintains the coordination to $O^{\delta 1}$ Asp12 but replaces $O^{\delta 1}$ Asp57 with $O^{\gamma 1}$ Thr86, moving away from Asp57. When the wild-type and mutant structures are superimposed (Fig. 6) it can be seen that the side chains of Asp57, Lys109 and Asp12 have moved. This is a consequence of the new hydrogen-bonding scheme and the displacement of Lys109.

4. Discussion

4.1. *N-capping and the reverse hydrophobic effect on CheY stability*

In two previous studies of mutating the N-cap residue for Asn (Bell *et al.*, 1992; Serrano & Fersht, 1989), the substitution was found to be destabilizing even though Asn is frequently found in nature at this position (Richardson & Richardson, 1988). In the latter paper the authors proposed that while Asn was a good N-cap residue it required a change in the backbone dihedral angles of the N-cap residue and that these changes sometimes resulted in strain or unfavourable contacts which destabilized the protein. The mutation of Phe to Asn in this work results in a large change in the side-chain $\chi 1$ angle from $-72°$ for the Phe residue in the apo structure to $\sim 180°$ in both mutants, but a very small change is observed in the backbone dihedral angles (Table 3). As this residue is highly exposed a large change in the-side chain torsion angle does not result in any unfavorable contacts. On the other hand, only a small adjustment in the φ/ψ dihedral angles is needed and, therefore, no destabilizing strain has been caused in the backbone and in fact the Phe14Asn mutation results in a large increase in protein stability [-12.1 kJ mol^{-1} (-2.9 kcal mol^{-1})] (Muñoz *et al.*, 1994).

In a previous thermodynamic and kinetic study (Muñoz *et al.*, 1994) and based on the three-dimensional structure for the mutation of Phe14 to Gly (Cronet *et al.*, 1995) it was suggested that substitution of this residue stabilized the protein through the inverse hydrophobic effect. In the inverse hydrophobic effect (Pakula & Sauer, 1990; Bowler *et al.*, 1993), substitution of a highly solvent-exposed hydrophobic residue by a more hydrophilic one increases the stability of the protein, because the hydrophobic residue is less exposed in the unfolded conformation. Recently, it has been found that a Phe14Ala mutation increases the stability only by -3.3 kJ mol^{-1} (-0.8 kcal mol^{-1}) indicating that the reverse hydrophobic effect can not account alone for the -12.1 kJ mol^{-1} (-2.9 kcal mol^{-1}) observed in the Phe14Asn mutation (López-Hernandez, Muñoz, Lacroix, Bruix, & Serrano, to be published). The crystal structures described in this work show that hydrogen bonding is playing a significant role as Asn forms an extremely good N-cap, bending over the helix cylinder without strain and without unfavorable interactions with neighboring residues. Moreover, we have found a forward–backward hydrogen-bonding pattern that resembles the local motif, termed capping box, commonly found at the N-terminus of α-helices in protein and peptides (Harper & Rose, 1993, Bordo & Argos, 1994) which could also cooperatively contribute to the stabilization of the protein in this mutant. In a capping box motif the side chain of residue $i + 3$ hydrogen bonds to the main-chain amide of the N-cap residue, while here it is the side chain of residue $i + 4$ that hydrogen bonds to the main-chain carbonyl group of the residue before the N-cap. We conclude that while the inverse hydrophobic effect contributes to the extra stability, in this case formation of the N-cap must also have a significant contribution.

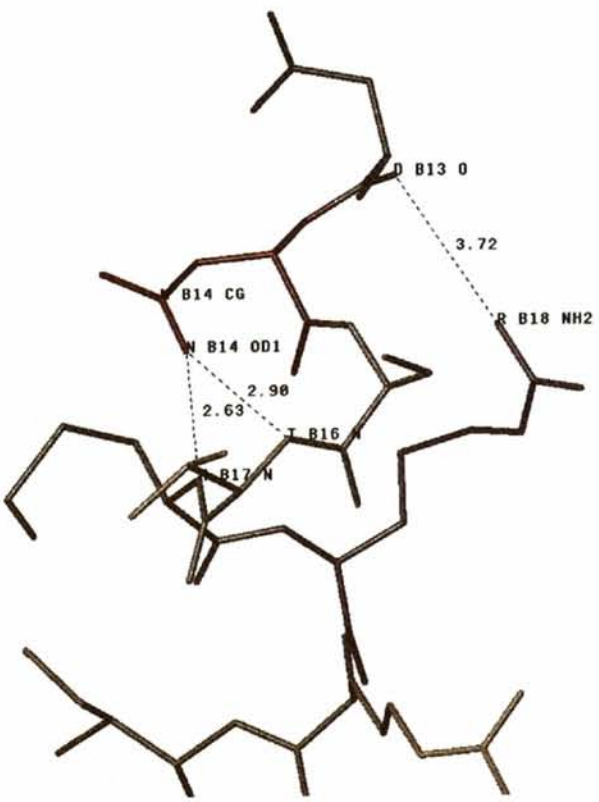

Fig. 4. Detail of the 'capping box' hydrogen-bonding pattern at the N-terminus helix $\alpha 1$ with mutation Phe14Asn. It indicates a bifurcated hydrogen bond from Asn14 to Thr16 and Met17 and a backward hydrogen bond between Arg18 and Asp13.

4.2. *Hydrogen bonds versus hydrophobic effect*

In order to be able to interpret the free-energy changes introduced by a point mutation in a protein it is necessary that the conformation of the protein does not change and that the mutated side chain does not make new interactions. In mutant 2, the hydrophylic Thr86 residue is accommodated due to the 110° rotation of the side chain. This allows the hydroxyl group to escape from a hydrophobic area and to form hydrogen bonds with Asp57 and an internally bound wate · molecule. There are compensating local movements in the surrounding area: (*a*) Asp57 and the water molecules move slightly while forming the new hydrogen bonds; (*b*) the side chain rotates into a nearby hydrophilic cavity which together with the displacement of the methylene side chain atoms of Lys109 partially fills this cavity. The final result is a very small destabilization of the protein, however it is not easy to extract any information regarding the importance of buried hydrogen bonds in protein stability from this mutant. More interesting is the case of mutant 1. In this case the side chain of Thr21 adopts the same conformation as Val21 in the wild-type protein and the residue is accommodated without producing any significant changes in the protein. As a result the carbonyl O atom of Met17 forms a bifurcated hydrogen bond with two hydrogen-bond donor atoms of residue Thr21: N and $O^{\gamma 1}$. Together with serine, threonine is frequently found establishing backward interactions in α-helices (Bowler *et al.*, 1993; Gray & Matthews, 1984) and this kind of hydrogen-bond pattern is no exception. The majority of side-chain-donor to backbone-acceptor hydrogen bonds are within the same substructure and, in particular, they consist of i to $i - 4$ interactions similar to the one described here (Stickle *et al.*, 1992). A similar backward i to $i - 4$ hydrogen bond was found in T4 lysozyme for the mutant Val75Thr (Blaber *et al.*, 1993). In this case the protein was destabilized by 5.4 kJ mol^{-1} (1.3 kcal mol^{-1}). In contrast, for the Val21Thr mutation in CheY there is no destabilization at all, only a change in the denaturation slope m. This change in m value is found in other Val to Thr mutations, suggesting that it could be due to the different solvation energies of Thr and Val (López-Hernandez & Serrano, 1996). The reason for the difference in stability for the same arrangement in CheY and T4 lysozyme, cannot be easily explained based on the crystal structures. It could be that small differences in the hydrogen-bond distance could explain this discrepancy, but with the present level of resolution we cannot support this hypothesis. Another possibility could be that the small conformational rearrangements (Met17) taking place around the

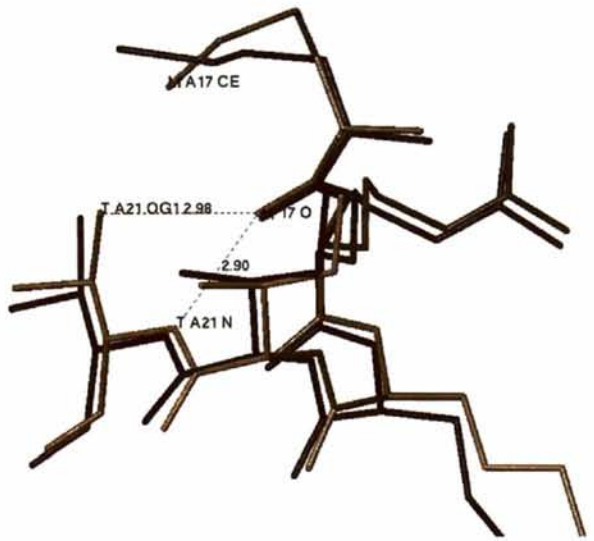

Fig. 5. Superposition of mutant 1 (this work) on the apo-CheY structure (pdb code 3CHY, Volz & Matsumura, 1991) at position 21. Yellow = mutant 1, molecule *A*. Purple = apo-CheY.

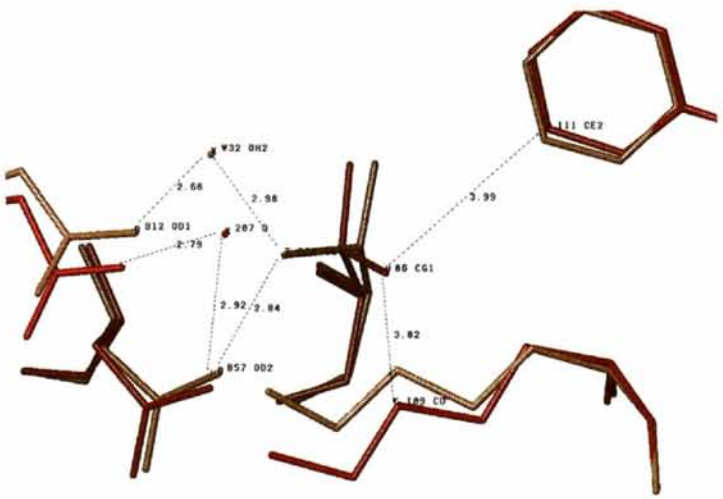

Fig. 6. Superposition of mutant 2 (this work), on the apo-CheY structure (pdb code 3CHY, Volz & Matsumura, 1991) at position 86 showing the rotation of Thr86 side chain and the subsequent change in hydrogen-bonding pattern. Yellow = mutant 2, molecule *B*. Pink = apo-CheY.

mutated residue in CheY are critical; for example, no displacement of the surrounding hydrophobic residues of the new O^{δ} atom (*i.e.* Ile100) were reported for T4 lysozyme. In conclusion, our results, together with those of T4 lysozyme, indicate that while burying the hydrophobic face of an α-helix should be destabilizing due to the unsatisfied hydrogen-bond potential of the helix carbonyl groups, the hydrogen bond made by the side chain of the buried Thr residue to the main chain of the helix partly or totally compensates for the burial of a hydroxyl group. We conclude that in certain cases, the loss in hydrophobic stabilization can be closely compensated by the gain in hydrogen-bond stabilization.

This work was supported by the Ministerio de Educación y Ciencia (grants PB92–0117 and PB95–0224) and the Centre de Referència en Biotecnologia (Generalitat de Catalunya). MP was supported by a short-term EMBO fellowship during her stay at the CID-CSIC.

References

Bell, J. A., Becktel, W. J., Sauer, U., Baase, W. A. & Matthews, B. W. (1992). *Biochemistry*, **31**, 3590–3596.

Bellsolell, L., Cronet, P., Majolero, M., Serrano, L. & Coll, M. (1996). *J. Mol. Biol.* **257**, 116–128.

Bellsolell, L., Prieto, J., Serrano, L. & Coll, M. (1994). *J. Mol. Biol.* **238**, 489–495.

Blaber, M., Linstrom, J. D., Gassner, N., Xu, J., Heinz, D. W. & Matthews, B. W. (1993). *Biochemistry*, **32**, 11363–11373.

Bourret, R. B., Borkovich, K. A. & Simon, M. I. (1991). *Annu. Rev. Biochem.* **60**, 401–441.

Bordo, D. & Argos, P. (1994). *J. Mol. Biol.* **243**, 504–519.

Bowler, B. E., May, K., Zaragoza, T., York, P., Dong, A. & Caughey, W. S. (1993). *Biochemistry*, **32**, 183–190.

Bruix, M., Pascual, J., Santoro, J., Prieto, J., Serrano, L. & Rico, M. (1993). *Eur. J. Biochem.* **215**, 573–585.

Brünger, A. T. (1992*a*). *X-PLOR, Version 3.1, a system for X-ray crystallography and NMR*, Yale University, New Haven, Connecticut, USA.

Brünger, A. T. (1992*b*). *Nature (London)*, **355**, 472–475.

Byrne, M. P., Manuel, R. L., Lowe, L. & Stites, W. E. (1995). *Biochemistry*, **34**, 13949–13960.

Creighton, T. E. (1991). *Curr. Opin. Struct. Biol.* **1**, 5–16.

Cronet, P., Bellsolell, L., Sander, C., Coll, M. & Serrano, M. (1995). *J. Mol. Biol.* **249**, 654–664.

Dill, K. A. (1990). *Biochemistry*, **29**, 7133–7155.

Filimonov, V. V., Prieto, J., Martinez, J. C., Bruix, M., Mateo, P. L. & Serrano, L. (1993). *Biochemistry*, **32**, 12906–12921.

Gray, T. M. & Matthews, B. W. (1984). *J. Mol. Biol.* **175**, 75–81.

Harper, E. T & Rose, G. D. (1993). *Biochemistry*, **32**, 7605–7609.

Kabsch, W. (1988). *J. Appl. Cryst.* **21**, 916–924.

Kraulis, P. J. (1991). *J. Appl. Cryst.* **24**, 946–950.

Laskowski, R. A., MacArthur, M. W., Moss, D. S. & Thornton, J. M. (1993). *J. Appl. Cryst.* **26**, 283–291.

López-Hernandez, E. & Serrano, L. (1996). *Folding Des.* **1**, 43–55.

Muñoz, V., Lopez, E. M., Jager, M. & Serrano, L. (1994). *Biochemistry*, **33**, 5858–5866.

Navaza, J. (1994). *Acta Cryst.* A**50**, 157–163.

Otwinowski, Z. (1993). *Oscillation data reduction program* in *Proceedings of the CCP4 Study Weekend: Data Collection and Processing, 29–30 January 1993*, edited by L. Sawyer, N. Isaacs & S. Bailey, pp. 56–62. Warrington: Daresbury Laboratory.

Pace, C. N., Shirley, B. A., McNutt, M. & Gajiwala, K. (1996). *FASEB J.* **10**, 75–83.

Pakula, A. A. & Sauer, R. T. (1990). *Nature (London)*, **344**, 363–364.

Richardson, J. S. & Richardson, D. C. (1988). *Science*, **240**, 1648–1652.

Rousell, A. & Cambillau, C. (1991). *Silicon Graphics Directory*, Silicon Graphics, Mountain View, California.

Santoro, J., Bruix, M., Pascual, J., Lopez, E., Serrano, L. & Rico, M. (1995). *J. Mol. Biol.* **247**, 717–725.

Serrano, L. & Fersht, A. R. (1989). *Nature (London)*, **342**, 296–299.

Serrano, L., Kellis, J. T. Jr, Cann, P., Matouschek, A. & Fersht, A. R. (1992). *J. Mol. Biol.* **224**, 783–804.

Shirley, B. A., Stanssens, P., Hahn, U. & Pace, C. N. (1992). *Biochemistry*, **31**, 725–732.

Stickle, D. F., Presta, L. G., Dill, K. A. & Rose, G. D. (1992). *J. Mol. Biol.* **226**, 1143–1159.

Stock, J. B., Stock, A. M. & Mottonen, J. M. (1990). *Nature (London)*, **344**, 395–400.

Stock, J. B., Surette, M. G., McCleary, W. R. & Stock, A. M. (1992). *J. Biol. Chem.* **267**, 19753–19756.

Volz, K. & Matsumura, P. (1991). *J. Biol. Chem.* **266**, 15511–15519.